Experimental Mechanics
DOI 10.1007/s11340-016-0152-3

Onset of Plasticity via Relaxation Analysis (OPRA)

A. Pandey[1,2] · R. Wheeler[3] · A. Shyam[1] · T.B. Stoughton[4]

Received: 5 November 2015 / Accepted: 3 March 2016
© Society for Experimental Mechanics 2016

Abstract In crystalline metals and alloys, plasticity occurs due to the movement of mobile dislocations and the yield stress for engineering applications is traditionally quantified based on strain. The onset of irreversible plasticity or "yielding" is generally identified by a deviation from linearity in the stress-strain plot or by some standard convention such as 0.2 % offset strain relative to the "linear elastic response". In the present work, we introduce a new methodology for the determination of the true yield point based on stress relaxation. We show experimentally that this determination is self-consistent in nature and, as such, provides an objective observation of the very onset of plastic flow. Our designation for yielding is no longer related to the shape of the stress-strain curve but instead reflects the earliest signature of the activation of concerted irreversible dislocation motion in a test specimen under increasing load.

Keywords Yield stress · Elastic limit · Yield surface · Microtesting · Mobile dislocation

✉ A. Pandey
dramitpandey@gmail.com

[1] Materials Science and Technology Division, Oak Ridge National Laboratory, Oak Ridge, TN 37831, USA

[2] Present address: Rolls Royce LG Fuel Cell Systems Inc., North Canton, OH 44720, USA

[3] MicroTesting Solutions LLC, Columbus, OH 43026, USA

[4] General Motors Research and Development Center, Warren, MI 48090, USA

Background

Plasticity in coarse grain alloys deformed at room temperature is controlled by dislocation motion induced primarily by activation of intragranular sources and subsequent multiplication processes [1]. At the same time, the concept of a yield stress is sometimes difficult to define because plastic deformation due to dislocation generation and movement is often a diffuse process rather than a singular event [2–4]. As a result, obtaining a clearly discernible transition from elastic to plastic strain within the flow curve, defining the concept of a "yield point", has proven elusive. The gradual transition from reversible strain to the irreversible strain associated with permanent dislocation movement in the stress-strain response has necessitated the common use of a 0.2 % offset strain definition of yield stress [4]. The 0.2 % offset definition is favored for most engineering design applications [5–7], and in particular, those applications that are not sensitive to the small plastic strains that occur at stresses below the 0.2 % offset definition.

In classical and advanced plasticity theories, the plastic behavior of a material in a general stress state is defined by an initial yield criterion (i.e. specifying the state of stress for the beginning of plastic flow), a kinetics of flow rule, and a hardening law. The onset of plasticity is often described by a definition of the elastic limit or yield point. These definitions are divided into small-scale (deviation from linearity, small offset, etc.) and more commonly used large-scale definition of yield (0.2 % offset, extrapolation, etc.) [8]. A strong interest in the design of lightweight systems, particularly in the automotive industry, has pushed the small scale definitions of yield point towards a more realistic lower limit and the ultimate goal would be the identification of the very earliest evidence of plastic deformation. The reason for this is that "springback", which is the change of shape of a stamped part as it is removed from the forming tools and trimmed, is caused by the

Published online: 17 March 2016

unloading of the forming or residual stresses and their associated elastic strains. It is necessary to predict this springback in order to minimize it early in the product design stage. And the prediction must be accurate to effectively compensate the tool shape early in the tool design stage in order to counter the inevitable amount of springback that cannot be minimized, so that the product shape relaxes to the desired design intent [9, 10]. The challenge of predicting springback in stamping of light weighting materials is exacerbated in comparison to products stamped from mild steels. For low density metals such as aluminum and magnesium alloys, the lower elastic moduli result in shape changes that are respectively 3 to 5 times higher than mild steel formed to the same level of stress. For advanced high strength steels, which can meet light weighting targets by reducing the material thickness while maintaining product strength requirements, the challenge is proportionally higher because of the higher forming stresses involved. The challenge of predicting and compensating for springback of these light weighting material options has brought into focus the fact the elastic strains that occur during forming are on the same order of magnitude as the 0.2 % offset plastic strain traditionally used in the definition of the yield stress, introducing a significant source of error in springback prediction, particularly in areas of the stamped part that are subjected to only a few percent plastic strain, where the elastic component is a higher percentage of the total strain. With traditional methods, which are based on 0.2 % offset yield stresses, springback prediction for light weighting metals is found to be unreliable, predicting sprung shapes that are centimeters different from reality, and requiring expensive trial and error modifications to the shape of the forming tools during the process of die tryout. These costs are exacerbated in the case of forming high strength steels, because harder tools, which are more difficult to re-machine, are required to form these metals. While other factors contribute to this large error in predicting springback, a more accurate definition of the onset of plastic strain, which would enable a more realistic decomposition of the total strain into elastic and plastic components, is expected to have significant improvements not only to reducing die tryout costs, but by detecting and correcting for springback early in the design process, will enable engineers to more efficiently design and optimize products for aesthetic appearance, fit and fastening of metal components, etc. [11–17]. Functional characteristics (crash performance, dent resistance, aerodynamics, model development, etc.) may also be improved with a more realistic decomposition of elastic and plastic strains, where many areas of the product see only elastic strains and the location of the elastic-plastic transition could be critical with respect to prediction of performance, especially in crash and dent resistance.

Recent studies employing microscale test specimens have adopted alternate definitions of yield stress, which are applied as a matter of necessity when large initial strain bursts are present [18–22]. These reports cite yield point values that range from apparent 0.2 % offset strain values, drawn from data showing large strain bursts, to values greater than 1 % offset strain, where plastic deformation has been arrested following an initial burst. However, these definitions are primarily used for material characterization or rough engineering purposes, and may not address the true elastic limit or true onset of plastic flow and irreversible deformation. In routine mechanical testing, forces are measured using some form of load sensor and most of the recent advancements in such testing have been in strain measurement. This progress has been driven by better strain resolution in time and/or length scales [23, 24], testing conditions and material geometry. At the same time, the existing definitions of the elastic limit/onset of yield remain subjective in nature, requiring determination of Young's modulus and/or strain level, or the assumption that some quantifiable deviation from the linear response implies yielding. These existing definitions make the definition of yield subjective, particularly for materials with high work hardening response which display non-linearity in the stress-strain response from an early stage [14].

Inaccuracies associated with such a subjective definition of yield could obscure relative contributions of the elastic and plastic deformation in the overall response. Many strain measurement techniques such as Electron Backscatter Diffraction, neutron diffraction or X-ray can be used to obtain improved local strain resolution within the gage section [12] of specimens. However, these techniques either lack sensitivity for the smallest of strains or are cost-prohibitive and/or challenging to implement, especially for testing under elevated temperatures and complex test conditions. As an alternative to these strain-based measurements, a stress-based probe of plasticity affords a highly sensitive window on the presence of dislocation activity.

The present work reports *in-situ* microtensile experiments where alternating stages of active loading and holding are utilized. During the holding segment, grip actuation is maintained constant and images of the specimen surface are recorded using a scanning electron microscope (SEM). During both the active grip displacement and hold stages, the load was recorded as a function of time, providing the data required in a classic stress relaxation experiment [25–37]. The resulting load-time history depends both on plastic properties of the specimen and elastic properties of the testing system and specimen. In general, during a fixed actuator displacement condition

$$\left(\dot{\varepsilon}_p\right)_{spec} = -\left(\dot{\varepsilon}_e\right)_t \tag{1}$$

where $\left(\varepsilon_p\right)_{spec}$ is the plastic strain in the specimen and $\left(\varepsilon_e\right)_t$ is the total elastic strain in the specimen and load train assembly.

This implies that any load relaxation detected by the load sensor is associated with a corresponding plastic deformation in the specimen. The plastic deformation in the specimen during stress relaxation can be correlated with the plastic (shear) strain rate in terms of mobile dislocation density

$$\left(\dot{\gamma}_{\mathrm{p}}\right)_{\mathrm{spec}} = \mathrm{b}\rho_m \mathrm{v} \tag{2}$$

where b is the Burgers vector of the mobile dislocations, and ρ_m is the mobile dislocation density and v is the dislocation velocity as a function of stress. Thus, under deformation conditions governed by dislocation glide, any non-zero strain rate exhibited during stress relaxation would be associated with dislocation motion. Stress relaxation behavior due to dislocation motion is commonly observed as a low strain rate which gradually diminishes over time. It is this fundamental correlation between irreversible dislocation motion and the corresponding change in stress during relaxation that forms the basis of the methodology proposed here for the accurate determination of the elastic limit.

The above discussion implies that in the event of near zero stress drop during relaxation tests in loading or unloading or reloading, the deformation in a specimen is purely elastic (or could be anelastic) i.e. with no plastic deformation in the specimen. With this background, we are proposing a new definition and methodology to measure the onset of plasticity in a metallic material that is based on stress relaxation. This new definition of onset of plastic deformation is stress based, and does not require measurement of strain and/or Young's modulus. In addition, it does not require a subjective analysis of stress-strain response such as the determination of the tangent point at the deviation from linearity in experimental data.

Experimental Methodology

Pure copper polycrystalline foil materials (designated, Cu-2 and Cu-10) with two different mean grain sizes (~2 μm and ~10 μm) and one polycrystalline specimen of Mg were investigated. The 10 μm grain-size Cu foil (Cu-10) was obtained by annealing as received 2 μm grain size foil (Cu-2) within an enclosed glass tube for 24 h at 850 °C and 1/3 atm. pressure containing a 4 % H_2/96 % Ar gas mixture. A combination of stencil mask, broad beam ion milling and focused ion beam (FIB) techniques [38, 39] was used to prepare the microtensile specimens. These microspecimens were fabricated in the shape of dogbones with one end attached to the bulk foil to remain fixed during loading while the other end remains free to be engaged by a movable pin during loading. The gripping or "free" end of the sample is large and flat relative to the specimen gage section with a hole at its center to allow the load pin to enter the opening. As in all mechanical tests, key alignments were maintained so that quantitative property measurements were possible. As in bulk tests, microscale tests can be susceptible to stress concentrations at the sample/grip contact surface. It has been shown that stress concentrations in the pin grip region can be mitigated by testing samples with gage sections much smaller than the pin contact area [39]. Thus, in the present tests employing a 30 μm pin, typical specimens had a gage section much smaller than the pin dimensions. Here, the gage thickness, width and length were 6 ± 1 μm, 12 ± 2 μm and 60–80 μm, respectively. SEM observations revealed typically four to five equiaxed grains in the through thickness direction for specimen Cu-2 while specimen Cu-10 exhibited a single grain through its thickness.

The copper and magnesium specimens were then tested in tension via pin loading using a micromechanical testing system in a large chamber SEM. In-situ microtensile testing was carried out using a piezoelectric actuated test frame configured with a 1N load cell (MTR-3 system from MicroTesting Solutions LLC, Columbus, OH, 43026, USA). Fully automated tensile experiments were conducted under stroke control in a Hitachi S-3400 SEM operating at 10 kV. The image resolution was held at 4000 × 1000 pixels and required about 30 s for each acquisition.

As noted earlier, the present tensile tests were carried out under nominally quasistatic conditions with alternating increments of loading and holding. However, it was observed that the assumption of an equilibrium state in the material during the image hold intervals was no longer valid at high stress levels. Under these stress conditions, load drops associated with relaxation were observed during the image acquisition hold periods and the stress measurements are not quasistatic. Thus, these tests must be considered interrupted or discrete loading tests. Short term relaxation (STR) test intervals lasting 30–40 s are present in the stress data collected during image acquisitions. Hence, many STR data sets are acquired during a single *in-situ* tensile test, one set per image. Long term relaxation (LTR) experiments, some lasting up to 30 min, were also collected by holding the load actuator stationary. Loading/unloading tests were also performed at various cross head stroke displacement intervals (see motivations below). Strains were measured using a MATLAB based digital image correlation technique [40–42] using images acquired during the short relaxation hold periods.

Results

Figure 1 shows uniaxial tensile stress-strain responses of two copper specimens a) Cu-2, a low work hardening ($n \sim 0.06$) copper foil with an average grain size of ~2 μm and b) Cu-10, a high work hardening ($n \sim 0.45$) copper foil with an average grain size of ~ 10 μm. These materials represent two distinct stress-strain responses for polycrystalline metals resulting from differences in initial dislocation density and grain size.

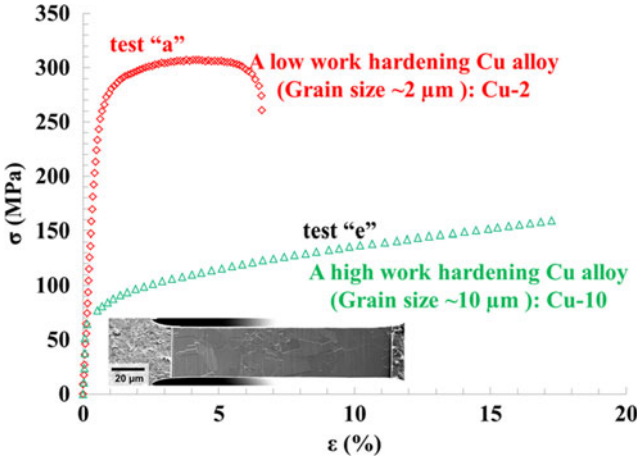

Fig. 1 Stress- strain response of Cu-2 (a low hardening alloy) and Cu-10 (a high work hardening alloy). Inset presents a typical SEM image showing the gage section of a microtensile specimen from the large-grain Cu-10 foil held under load. Subsequent images are recorded as the sample is loaded to different levels of stress and are used to measure strain

While the stress values shown in Fig. 1 are part of a continuous data stream recorded during each test (Fig. 2), the strain is measured from discrete SEM images giving rise to the distinct data points. In a previous report, the strength measured in these samples is in close agreement with macroscopic tests conducted on similar materials [39].

Figure 2a and b show the step-wise stress-time responses of Cu-2 and Cu-10 specimens, for a series of discrete load/hold experiments. Here, loading increments are associated with the nearly vertical segments of the curves. The holding increments (during image acquisition) are associated with nearly horizontal segments in the elastic regime. Then, at high stresses in the range of 250 MPa for Cu-2 and 90 MPa for Cu-10, the displacement hold increments are accompanied by a drop in stress with time. This stress drop at nearly constant displacement is the result of relaxation. The STR experimental data is associated with the 30–45 s hold conditions required during image acquisition. Tests in Fig. 2 were conducted with different incremental displacement between imaging hold states. In the present tensile tests, different crosshead displacement ramps were used to vary the magnitude of the incremental stroke between successive images (i.e. the stroke moved by the actuator between images, typically 0.5–2 μm). The strain in the sample is much less due to compliance of the load train. For example, in Fig. 2a, tests "a", "b" and "c" had discrete strain increments between SEM imaging hold states of 0.025, 0.014 and 0.063 μm, respectively. The nominal strain rate during active loading ramps was held constant across all tests at about 10^{-4} s^{-1}. Figure 2 also includes LTR experiments that were performed using the Cu-2 and Cu-10 specimens after significant plastic deformation was introduced in selected tests. Similar to STR experiments, LTR experiments show higher load drop for the Cu-2 specimens (i.e. ~10 %) as compared to the Cu-10 specimens where load decays up to ~5 % from its initial level. These tests also include unloading-reloading sequences where the stress is systematically decreased and then increased in the "V"-shaped sections of the curves. These unloading cycles illustrate that the relaxation process can be halted by reductions in stress and reactivated upon increasing stress. This confirms that the response is related to the material behavior and not to any testing artifacts.

A linear slope ("m" with units of MPa- min^{-1}) was calculated for every STR window to study the loading, unloading, and reloading response of Cu-2 and Cu-10 specimens. A negative stress-time slope indicates relaxation straining is underway where sample elongation occurs as the stroke is held fixed. A near zero slope indicates a stable specimen geometry where the sample length remains nearly constant under load as the stroke is held constant. An initial non-zero slope is thought to be related to thermal effects experienced by the strain gage based load cell or the piezoelectric actuator. Selected stress-time data from Fig. 2, showing imaging hold time

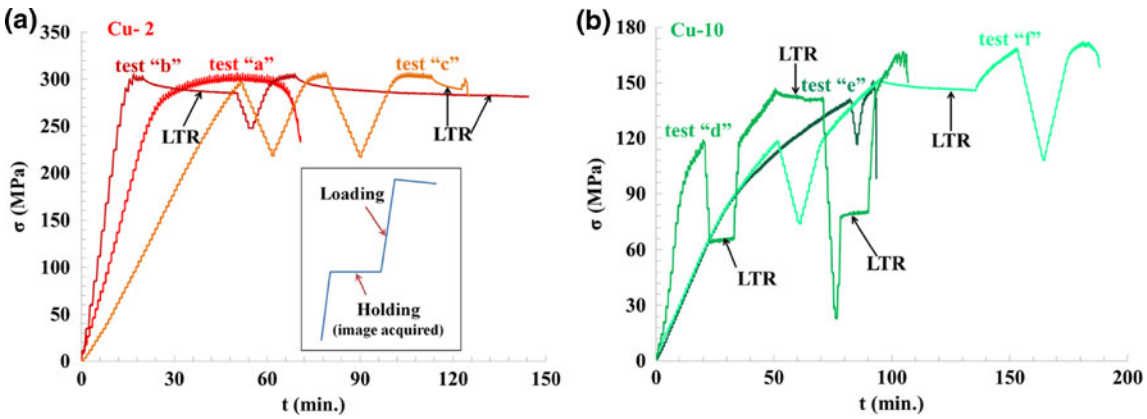

Fig. 2 (**a**) Stress- time response of fine grained Cu-2 microsample tensile tests. Different loading strains are used between hold increments for the three tests. The strain rate during all loading stages is 10^{-4} s^{-1}. The short holding segments occur during SEM image acquisition and correspond to Short Term Relaxation (STR) measurements while the Long Term Relaxation (LTR) data is found from the extended hold periods indicated. (**b**): Stress- time response of large grained Cu-10 microsample tensile tests (see Fig. 2a comments)

windows alone, are plotted in Fig. 3a and b (left ordinate) for *in-situ* tests "c" and "f", respectively. The results for both experiments show linear slope values (right ordinate) near zero throughout the early stages of loading. These slope values sharply change to negative values beyond some elevated level of stress during subsequent loading. However, the negative values of slope abruptly return to near zero upon unloading (e.g. at 52 min. in Fig. 3a). The linear slope remains close to zero throughout the unloading cycle and into the reloading interval until again returning to negative values as the stress in the specimen approaches the initial unloading level. The insets of Fig. 3 show the qualitative relaxation response during an unloading-reloading cycle in the copper foils reported here. Such loading-unloading-reloading curves have been used to propose the concept of yield surfaces and its evolution with plastic deformation [42].

The dislocation activity underlying the relaxation phenomenon exhibited in our *in-situ* discrete loading experiments is dependent on the crystal structure and nature of deformation in the material being tested. *in-situ* microtensile tests were also conducted on a polycrystalline Mg specimen. Here, the hexagonal close packed (hcp) crystal structure is combined with multiple available deformation modes, including dislocation slip and twinning, present a class of material distinct from face centered cubic (fcc) copper.

Figure 3c shows the stress-time and first derivative, "m", of the stress-time behavior of a 99.9 % pure Mg specimen. As in the Cu tests (Fig. 3(a) and (b)), the general features of the relaxation slope throughout the test include (i) a near zero slope on initial loading, (ii) a transition to negative slope with increased load and (iii) the return to near zero slope on unloading. Unlike the Cu tests, the Mg specimen showed slightly negative slope at all times and significant relaxation persisted during initial *unloading*. It does return to near zero levels but only with significant unloading. There was a nearly immediate transition to zero slope in Cu alloys at the onset of unloading. On reloading, negative slopes are found for stress levels well below the initial unload stress in contrast to the case of Cu-2 and Cu- 10. These observations have particular importance in modeling plastic deformation, suggesting that in the case of the Mg alloy, the yield surface is not constrained to keep up with the current stress state, but lies somewhere

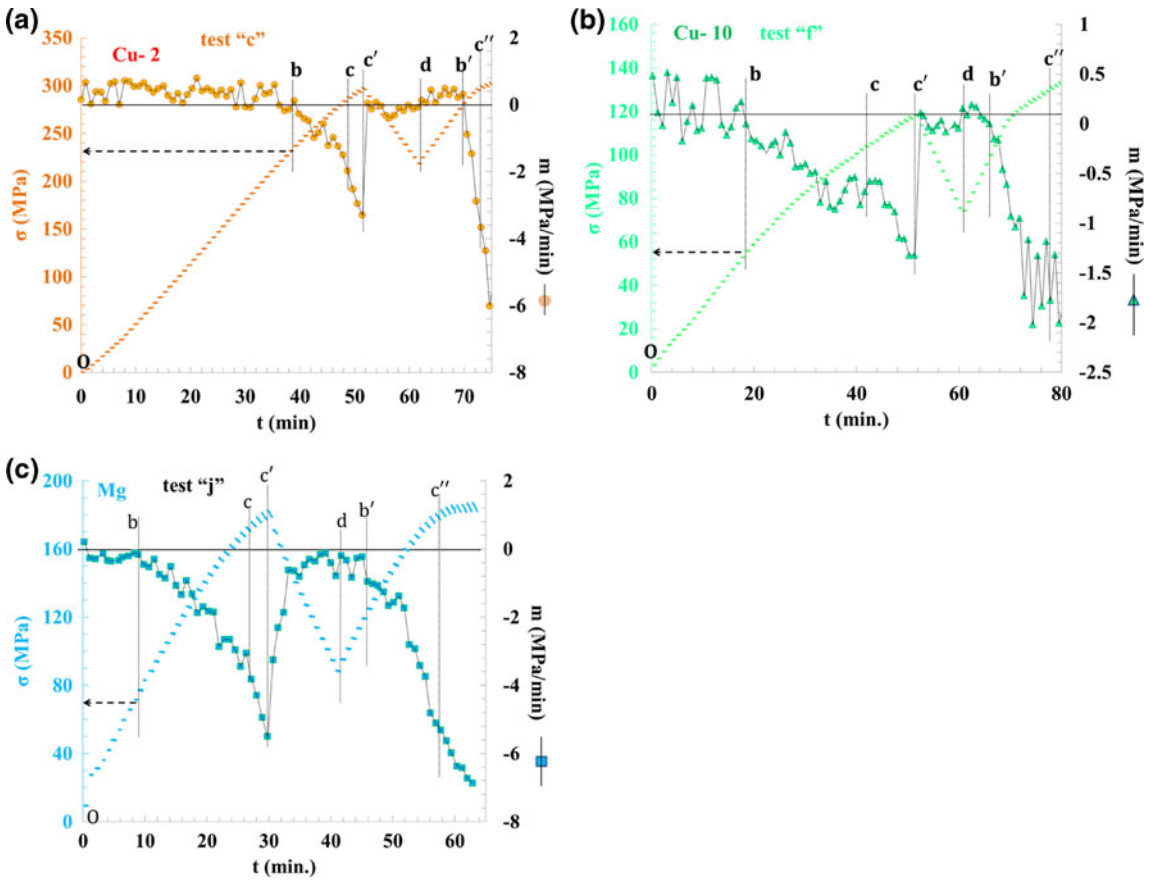

Fig. 3 (**a**) Data from Cu-2 microtensile test "c" in Fig. 2a showing stress-time response during hold stages along with the slope (*circles*) measured for each discrete stage. (**b**): Data from Cu-10 microtensile test "f" in Fig. 2b showing stress-time response during hold stages along with the slope (*triangles*) measured for each discrete stage. (**c**): Data from Mg microtensile test "f" showing stress-time response during hold stages and the slope (*squares*) measured for each discrete stage

below, at the stress level when the slope during relaxation goes to zero. The remaining σ-t curves for Cu-2 and Cu-10 samples in Fig. 2 were analyzed in the same manner described for Fig. 3 to determine the slope in stress during every hold stage. Each test was conducted with a different incremental displacement interval between relaxation hold stages corresponding to a unique global strain rate for an individual experiment. The slope data for the Cu-2 and Cu-10 samples were then re-plotted as stress versus negative relaxation slope in Fig. 4a and b, respectively. These plots present the slope data in decreasing magnitude since the relaxation begins near zero during initial elastic loading, when relaxation is not active, and decreases at high stresses when significant plastic flow is present. The transition from non-relaxation, zero slope behavior during elastic loading to relaxing, negative slope behavior was found to be consistent for a given copper grain size. In Fig. 4, where tests have different displacement magnitudes between STR hold intervals, the transitions from near-zero STR slope to negative slope in the Cu-2 and Cu-10 specimens were found to occur at about 242 ± 1 MPa and 58 ± 2 MPa, respectively. We propose that these values correspond to a transitional condition where plastic flow has been activated somewhere within the sample as stress is increased. The transition to negative slope demarks an onset of relaxation behavior directly correlated to an onset of plasticity. This gives rise to a new determination of yielding related only to the activation of irreversible flow in a metal, a measurement of the Onset of Plasticity via Relaxation Analysis (OPRA).

At this point, we have illustrated how a linear slope approximation to the relaxation response during hold intervals in microtension tests can be performed. These enumerated values then lead to some form of demarcation between deformation regimes, commonly considered as the elastic and plastic regions, of the stress-strain curve. Relaxation behavior is generally understood within the context of irreversible dislocation motion in the presence of stresses sufficient to maintain plastic flow in a test specimen. Additional tests (Fig. 5) were conducted that provide insight into the movement of dislocations near the yield point in polycrystalline metals. Through controlled loading-unloading experiments, it is possible to distinguish contributions of both reversible and irreversible dislocation motion to the global strain in a test specimen. These have been used to study the strain response of metals where slow recovery of total strain can be accomplished through purely elastic recovery combined with the reversible, time-dependent defect movement underlying anelastic strain [1].

Three loading-unloading experiments were conducted on a Cu-10 specimen, achieving maximum stress levels that were either (i) within the elastic or (ii) within the plastic deformation regime for that material (based on Figs. 2(b) and 3(b)). In Fig. 5(a), the microtensile specimen was loaded at the same stroke rate as all previous tests but the stroke range between holds was large (2 μm step). This rapid loading was reversed when the stress reached about 46 MPa, i.e. below the true elastic limit of 59 MPa for Cu-10. The sample was then slowly unloaded using small displacements of 0.2 μm between hold intervals. Upon complete unloading, the strain measured near zero. Additionally, throughout unloading, the strain corresponded to precisely the same stress value as during loading, exhibiting fully reversible response. Figure 5(b) presents the test where loading of the sample progresses as in Fig. 5(a) with a small additional hold period at the maximum load. During this interval, several images were collected but no movement of the load train occurred. Then a rapid unloading sequence (5 μm step) was undertaken until the specimen was completely unstressed. While unstressed, images of the microspecimen were periodically collected for the same time duration as in the previous experiment. Unlike the prior test, the strain in the specimen continued to change upon complete unloading as indicated by the blue diamond data points in Fig. 5(b). The figure inset shows the hysteresis in

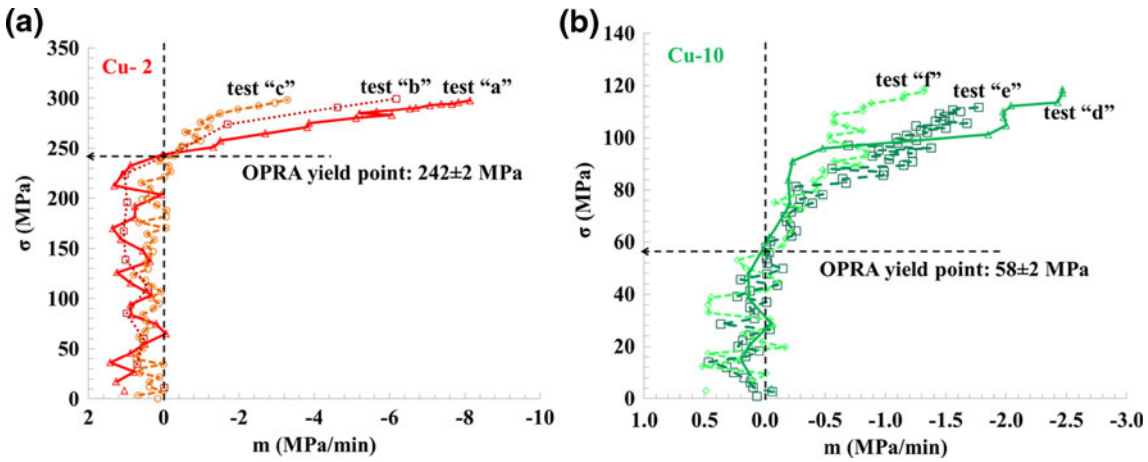

Fig. 4 (**a**) Plots of stress versus hold stage slope for early hold windows during microtensile tests of Cu-2 specimens shown in Fig. 2a. (**b**): Plots of stress versus hold stage slope for early hold windows during microtensile tests of Cu-10 specimens shown in Fig. 2b

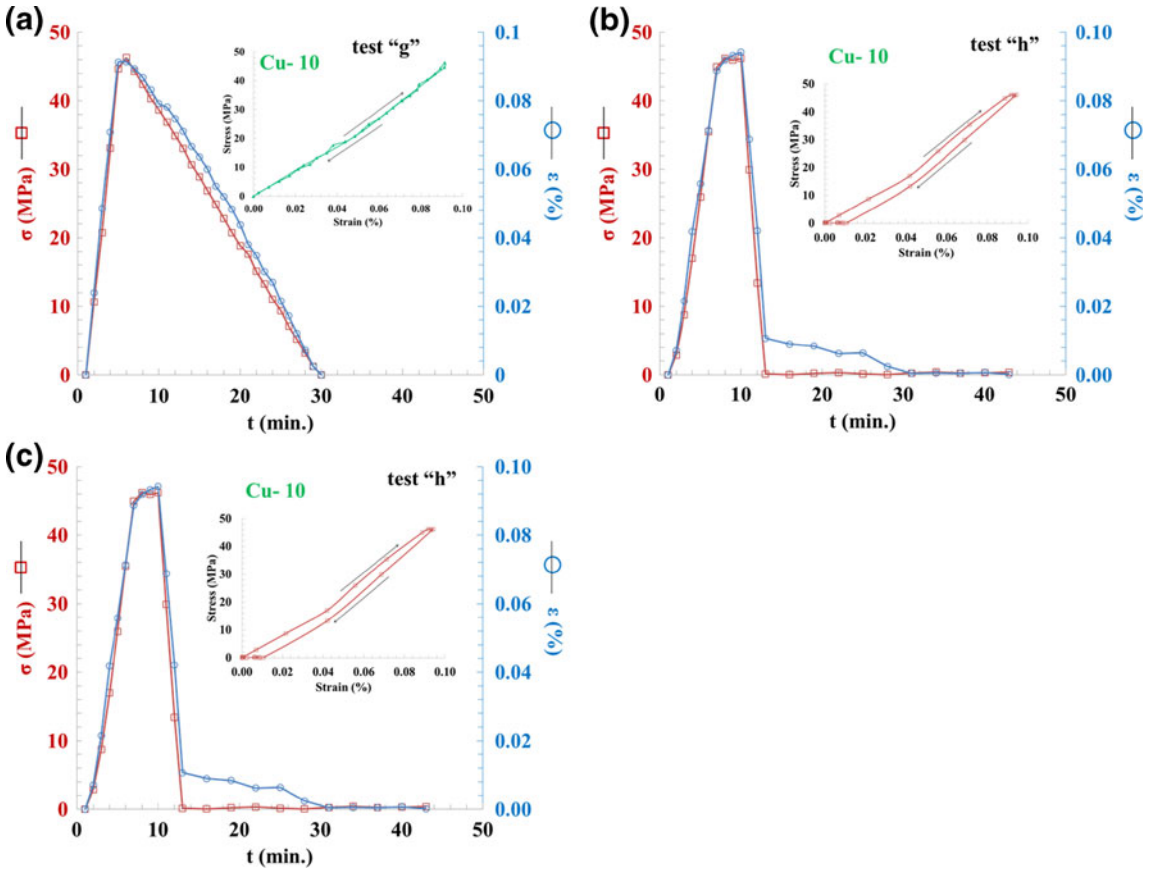

Fig. 5 (**a**) Stress-time response (*squares*) and strain-time response (*circles*) for a Cu-10 sample loaded rapidly to a maximum stress (46 MPa) below the OPRA yield point (58 MPa) and then unloaded slowly. Inset shows the stress-strain curve for this load-unload test. (**b**): Stress-time response (squares) and strain-time response (*circles*) for a Cu-10 sample loaded rapidly to a maximum stress (46 MPa) below the OPRA yield point (58 MPa), held for 4 min and then unloaded rapidly. Inset shows the stress-strain curve exhibiting hysteresis associated with anelastic, recoverable strain as recently demonstrated for fine grained aluminum [1]. (**c**): Stress-time response (*squares*) and strain-time response (*circles*) for a Cu-10 sample loaded rapidly to a maximum stress (81 MPa) above the OPRA yield point (58 MPa) and then unloaded rapidly. Inset shows the stress-strain curve for this load-unload test which includes extensive plastic flow as well as anelastic strain recovery

the stress-strain plot associated with the slow time-dependent recovery of the gauge length to its original dimensions. In Fig. 5(c), the stress time response is shown for a third test of the sample, which has clearly exceeded the true elastic limit and the 0.2 % offset yield point. The maximum stress in this third test of the sample has clearly exceeded the true elastic limit and was well above the 0.2 % offset yield point. The sample was then unloaded abruptly to zero stress from the high stress state after significant plastic flow occurs. This ensures maximum time-dependent strain recovery upon full unloading. As in Fig. 5(b), Fig. 5(c) also shows a continued strain recovery, i.e. anelastic strains or viscoelasticity. This reversible anelastic strain retrieval in our large-grained copper material requires time duration of about 20 min. The large residual strain that remains is associated with irreversible plastic deformation accumulated during loading beyond the yield point. Similar observations on the hysteresis during loading and unloading were recently reported by *Rajagopalan* et al., [1].

In a more conventional manner, evidence of an onset of plasticity related to irreversible dislocation motion may be found in the image data recorded during the discrete loading tests. Figure 6a presents a portion of the stress-strain curve for a Cu-2 sample where strain has been measured from DIC analysis of individual images, as done for Fig. 1. This plot includes the initial elastic response and the transition into the plastic region of the curve. Discrete load values for 31 data points have been recorded at the onset of image acquisition with the image numbers for several points indicated along the curve. In Fig. 6b, stress-time data corresponding to times in the vicinity of the onset of relaxation are shown with approximated slope lines for the image hold periods. The image numbers correlate this curve to the images designated in the stress-strain data of Fig. 6a. The transition from slightly positive slope (gold line) to definitively negative slope (purple line) takes place at image 26. Any significance in the incremental strain measured from images 25 and 26 is not directly evident in the stress-strain plot of Fig. 6a. Indeed, any

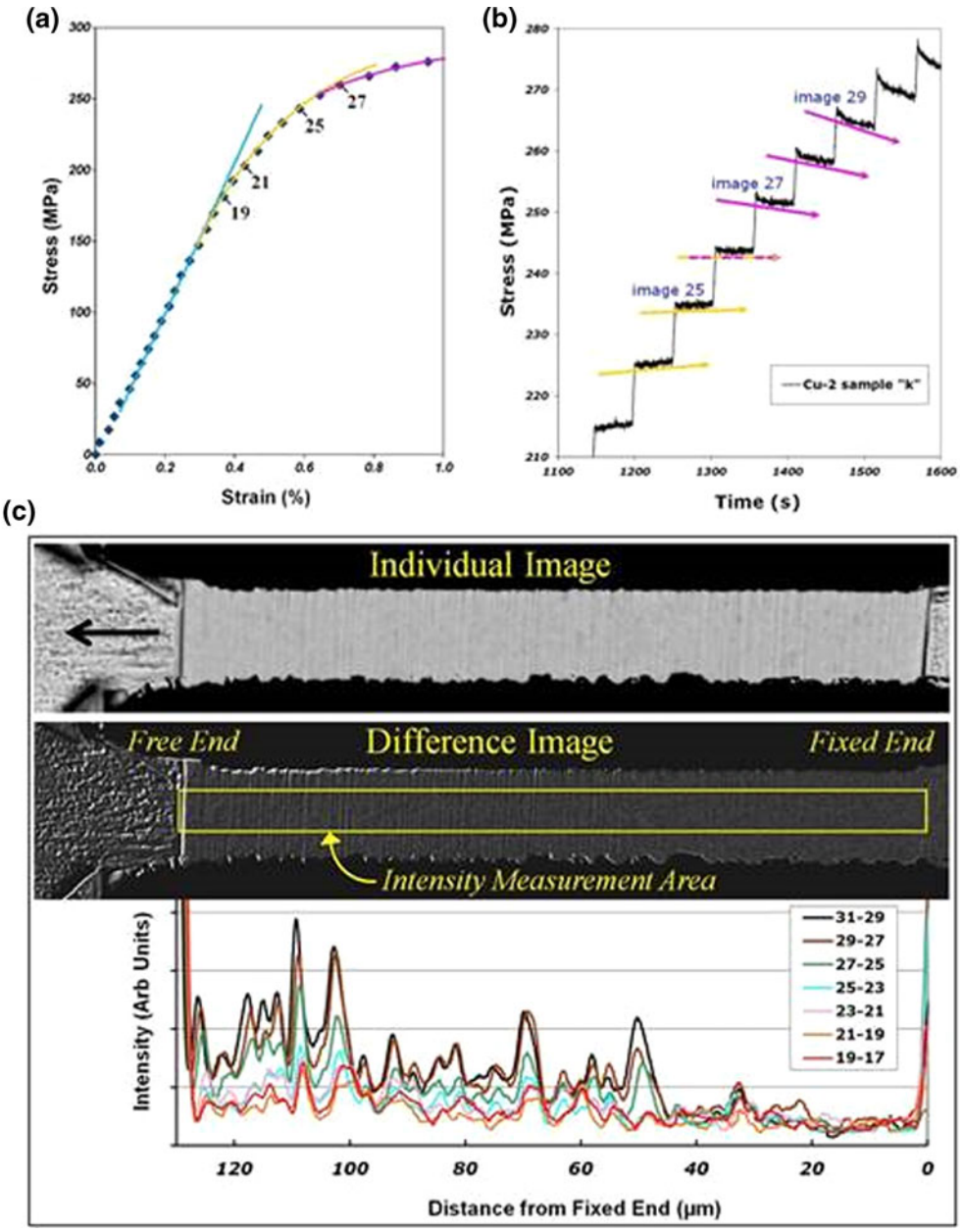

Fig. 6 Images analysis and stress- strain response of Cu 2 test "k" (**a**) Early response where selected image frame numbers are indicated near key data points, (**b**) Relaxation slope analysis near "yield point" and (**c**) Difference Image analyses for images near "yield point" including a typical starting image and the Difference Image calculated by simple subtraction of one image pixel intensity from another (see text). Intensity plots show variation in average pixel intensity as a function of distance from the aligned end of the test specimen (*right side*)

determination of a "yield point" from such a curve alone would require some form of subjective interpretation of the curve from about point 19 through point 27 and beyond.

As noted in the introduction, the onset of plastic deformation is generally considered as a discrete event rather than a continuum response. Thus, a critical dislocation source can be activated and dislocation multiplication and propagation ensues. Such a mechanism leads to local plastic deformation in polycrystalline microscale specimens like those fabricated from the present copper foils. Since the entire gage section of the microtensile specimen has been visualized in the current tests, a simple Difference Image (DI) analysis can be used to identify localization of deformation [39]. It is then possible to compare the earliest observed plastic deformation deduced from this image analysis with the observed onset of relaxation.

Figure 6c shows a single secondary electron image taken from the series used in Fig. 6a (image 27). In these images, the right side of the specimen is fixed to the bulk foil while the left or "free" side is engaged by the loading pin grip during testing. This individual image has been specifically aligned with a similar image from an earlier hold interval (image 25) so that their right sides are in best registry. A DI was then calculated from the two aligned images in Fig. 6c. For this DI, little contrast and relatively low intensity results when microstructural features are similarly oriented within the two starting images (i.e. as in the aligned right side). Microstructural

features on the left side of the images are less well aligned as a result of different strain experienced in the sample for the two images. Hence, the left side of the gage section represented in the Fig. 6c DI exhibits more contrast than the right. This contrast reflects the pronounced FIB curtains developed in this particular microtensile specimen during processing, where more surface roughness is present than is generally desired.

A semi-quantitative analysis of the DI intensity variation along the gage length has been carried out using the average intensity within the overlaid box shown in Fig. 6c. A 5 × 5 pixel top-hat smoothing function was applied to the box area prior to calculating the average vertical intensity along the entire 3200 pixel gage length. Incremental DIC strain measurements determine global displacements of only 2 pixels along this full 3200 pixel length between two subsequent images acquired within the elastic loading regime. In this situation, localized strain along the loading direction (ε_{xx}) can be more easily visualized using the 1-dimensional DI intensity plot shown at the bottom of Fig. 6c. Here, the average DI intensity is sensitive to axial strain, ε_{xx}, because the aligned FIB surface features ("curtains") are nearly perpendicular to the strain. The DI signal intensity can be further enhanced by using every other image when carrying out the measurement, thus increasing the magnitude of strain between image pairs used in each subtraction. We have used alternate odd images for this purpose. From the DI intensity plots, we note that the curves fall into two categories. One category, including DI curves 25–23, 23–21, 21–19 and 19–17, shows a gradual increase in magnitude from the fixed end of the sample to the free end (right to left) of the gage length at 120 μm. Variations about this gradual trend are small throughout the entire gage section. The second category of DI intensity variation includes curves 31–29, 29–27 and 27–25. Here, the intensity shows similar gradual increase from the fixed end to about 45 μm, at which point, the intensity is dramatically increased relative to the curves associated with the earlier DI measurements. The variation above the minimum values (i.e. peak to valley) is also markedly increased from 45 to 125 μm. This interpretation provides a quantitative determination of the position of plastic strain within the test specimen but does not return an accurate magnitude of that deformation. More importantly, it provides an alternate method to determine the stress at which irreversible dislocation flow begins. That stress is associated with images 26 or 27.

Discussion

As seen in Fig. 1, the identification of the onset of plastic flow from stress strain data is not obvious for some metals and microstructures, such as Cu-10. Here, anelastic strain obscures the identification of the onset of plastic flow and its non-recoverable deformation. A sharper transition from linear elasticity to plastic flow is evident in the Cu-2 samples and this behavior might allow a more readily available measure of the yield stress. Nevertheless, a common definition of yield based on the physics of plastic flow that would apply to crystalline materials in general is desirable. At the same time, a viable measurement methodology that addresses this definition and is applicable to various materials is important.

As evidenced by the limited *in-situ* experiments reported here in materials of both similar (i.e. Cu-2 and Cu-10) and dissimilar nature (i.e. Cu and Mg), the differences in stress-strain behavior often call for different ways to define and quantify yield [5, 8]. However, all definitions of yielding seek to somehow distinguish between elastic and plastic behavior. The elastic response of a material under an applied stress can then be further differentiated into purely elastic and anelastic contributions, where the latter is associated with reversible dislocation motion. It is the ability to discern irreversible dislocation motion alone that forms the basis of the present definition and test methodology to identify the true yield point. Similar *in-situ* SEM experiments exhibiting relaxation behavior were recently reported elsewhere [39–41, 43]. However, in one case, the load drops associated with relaxation strain were considered an experimental artifact impeding quantitative strain measurements. Stress/load relaxation experiments have been used extensively to study activation energy and activation volume [26, 32–34], dislocation velocity/density [25–33, 35] and internal stresses [26, 28, 35–37] in metals and alloys at room and elevated temperatures.

It is observed in the initial stress relaxation experiments shown in Fig. 2 that there is no stress relaxation in hold periods during early loading until the stress rises above a critical level, in Cu samples of different grain size. Since stress relaxation is indicative of irreversible plastic flow, it is argued that the observation of the onset of stress relaxation observed in these hold tests while progressively loading the specimens is an objective way to define the initial yield. It is also noted in Fig. 2 that after exceeding the stress where relaxation first occurs, that stress relaxation is not found during unloading hold intervals. This is consistent with conventional plasticity theory of strain hardening materials, in which the yield stress increases with plastic strain. It is then argued that this same method can be used to track the evolution of the yield surface. This argument is consistent with the additional observation that upon reloading both Cu specimens with different initial grain size, stress relaxation is not observed until the stress rises to the level achieved prior to the last unloading.

An analytical method is described in which the stress relaxation is first characterized by measuring the slope of the stress-time data during discrete hold intervals, as presented in Fig. 3. This quantitative analysis provides a more detailed view of the transitions between the elastic and plastic deformations discussed in reference to Fig. 2. It is seen that the experimental calculation of the slope parameter, m, hovers

about a value of zero during initial loading, indicating the absence of relaxation for a stress condition in the elastic state. The slope then drops to negative values in the presence of plastic flow induced by higher applied stresses. The magnitude of the slope increases with the magnitude of the stress after yielding, suggesting a connection between the dislocation structure/density and the resistance of the material to plastic flow. Based on these results, it is reasonable to assume that the stress level reached after each hold period is indicative of the true quasistatic stress-strain response of a material only within the elastic regime [44].

The transition from elastic/anelastic to plastic flow defined by the linear slope criterion shows that the true OPRA for Cu-2 and Cu-10 is independent of the loading and strain rates, as shown in Fig. 4a and b, respectively, for discrete loading rates. The insensitivity of the end of the elastic/anelastic response to the stress and strain rates is consistent with the hypothesis that the onset of stress relaxation provides an accurate definition of the true beginning of plastic flow. Thus, the OPRA for samples Cu-2 and Cu-10 are found to be 242 and 58 MPa, respectively. That this true onset of plasticity/yield point is related to the irreversible motion of mobile dislocations is supported by observations for Cu-10 in Fig. 5 where: (i) *reversible* dislocation movement alone (anelastic behavior) is found below the 58 MPa true yield stress and (ii) full recovery of strain is not found after the same specimen is further loaded above 58 MPa due to the presence of significant *irreversible* plastic flow. In addition, the presence of reversible dislocation activity both below and above the true yield point is indicative that the onset of relaxation is directly related to the irreversible and only the irreversible dislocation motion.

The prominent increase in Difference Image intensity throughout the free side of the gage section isolates the stress level where concentrated plastic strain is first observed. Local image displacements are much more evident in images 27, 29 and 31 than in any image recorded at lower stresses in Fig. 6a. Plastic deformation therefore begins in image 26 or 27 and is then propagated in subsequent images 29 and 31. This localized strain from the DI analysis can be directly correlated with the permanent deformation underlying the relaxation observed in the first clear negative slope of Fig. 6b. The subtle interpretation of the relaxation slope in image 26 and the difficulty in interpreting the DI intensity when that image is interpreted are left for later analyses. The key observation is that both relaxation (Fig. 6b) and direct strain observations (Fig. 6c) concur in identifying the onset of plastic strain in this test at approximately 245 MPa.

There is excellent correlation between the onset of relaxation and observation of a marked increase in the intensity of the Difference Image, both defining the Onset of Plasticity (OP) where irreversible dislocation motion commences. The quantitative interpretation of the shape of a stress-strain curve is less complex when the determination of the OPRA is at hand. Below the OPRA, the stress-strain response exhibits both elastic and anelastic strain components. In our present example for the Cu-2 foil specimen, the shape of the stress-strain curve in Fig. 6a deviates from linearity somewhere near images 17 through 19. Below this stress (about 160 MPa), nearly pure elastic behavior is exhibited as indicated by the blue line. Within the data range from image 19 to image 26, the combined elastic and anelastic responses account for the curved shape of the stress-strain behavior highlighted by the yellow curve. Then, the OPRA defines the region of the curve dominated by plastic flow beyond the stress at image 26 (approximately 245 MPa). While identification of elastic and anelastic strain contributions is somewhat subjective, the determination of the OPRA is clear from the relaxation slope analyses found in Fig. 4a and b.

We also investigated this method applied to a Mg sample and compared this to the Cu material. As noted previously, in the case of copper, we showed evidence in Fig. 3 that stress relaxation, and by proxy, plastic flow, ceases nearly immediately at the start of unloading, and does not recommence until the stress is increased again to the level achieved prior to the last unloading. This is consistent with classical plasticity theory in which the yield surface moves with the applied stress condition and remains at that level if the stress drops into an elastic state. It was also observed that the initial yield stress of the Cu samples is found to be near the point of departure from linear elasticity, as seen in Fig. 3a and b. Similarly, as seen in Fig. 7, the Mg sample also shows clear transitions between (near) zero and finite relaxation, and so, as in the case of copper, the active relaxation state is linked to dislocation activity and plastic flow. However, the details of this behavior in Mg show significant differences when compared to the Cu discrete hold relaxation response. Onset of relaxation for our Mg sample occurs at a stress level well below what appears to be the linear domain during initial loading. Furthermore, during unloading, relaxation continues for an extended drop in load indicating persistent plastic flow. At some significantly lower level of stress (approaching 50 % of the initial unloading stress), the relaxation disappears, indicating cessation of plastic flow during the hold interval. Consequently, unlike copper, after initial yielding, the yield surface for Mg appears to significantly fall behind the increasing level of stress, as suggested in the schematic illustration in Fig. 7, with the stress conditions, b, c, etc. corresponding to the denoted stress conditions indicated in Fig. 3a, b, and c. Also, like the Cu materials, on reloading the Mg from the elastic state, stress relaxation is observed to resume when the stress reaches the level at b', which is the about the same level of stress during the prior unloading between points c' and d at which stress relaxation disappears in Fig. 3c.

We should also make it clear that, whereas this definition of initial yielding is objective and not subjective as are other

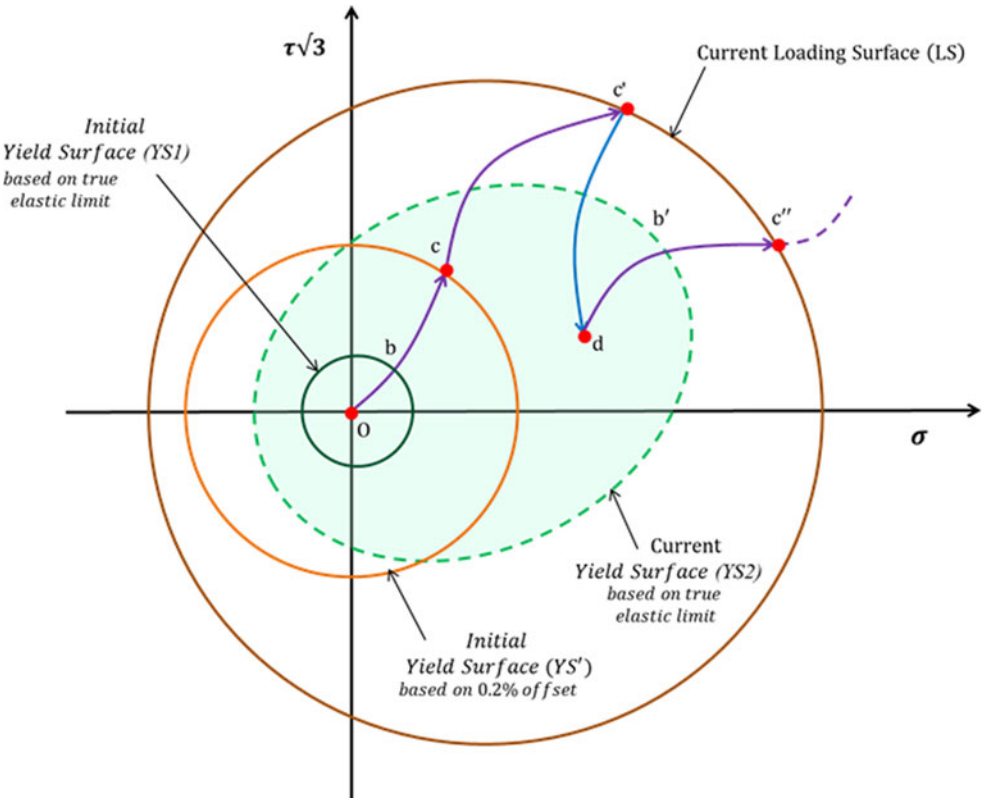

Fig. 7 Schematic of initial yield surface (based on 0.2 % offset strain and true elastic limit), loading surfaces and current yield surface (based on true elastic limit). The points labeled b, c, c', d, b' and c" correspond to the stress and strain states identified in the experimental data shown in Fig. 3a, b, and c. Note: The initial yield surface and current loading surface are based on von-Mises criterion

currently employed definitions, the hardening and subsequent yield behavior appear to be more complex. While the yield surface appears to be close to the loading surface for the Cu alloys, where stress relaxation is not observed during the first increment of unloading, this is not the case for the Mg alloy. We are not trying to provide solutions to modeling the hardening behavior of polycrystalline metals in this paper, but instead point out that realistic solutions will not be expected until it is possible to accurately decompose the experimental elastic and plastic components of the deformation. From the experimental evidence shown here, this decomposition is now possible using an objective determination that is based on the physics of plastic deformation. Use of this definition now allows measuring the stress giving rise to initial plastic flow at high temperatures and in harsh environments without the need for strain measurements.

The present tensile tests were conducted at room temperature where the homologous temperature, T/T_m, is 0.22 for copper and significantly higher, 0.33 for magnesium. Deformation mechanism maps, such as those presented by *Frost and Ashby* [44], detail a variety of deformation modes that may govern the relaxation observed in the current discrete loading tests. The relaxation response at a given stress level and temperature will be dependent on the deformation regimes available for the particular test conditions. At elevated temperatures, different creep mechanisms will influence the non-equilibrium relaxation behavior even at low stress levels. Nevertheless, the onset of plasticity due to activation of dislocation glide during incremented loading will always be associated with a marked increase in the magnitude of the negative slope in the initial stress relaxation. Thus, the load drops observed during the image hold stages of the present pseudo-quasistatic tests reflect only the initial, most rapid relaxation response. At lower homologous temperatures, deformation in copper is expected to be limited to elastic and plastic modes alone while magnesium may exhibit low temperature creep at high stresses. Through consideration of their deformation mechanism maps, the creep response available in the Cu and Mg tests presented here will not be evidenced in the short term relaxation data. Thus, at ambient temperatures, relaxation in Cu and Mg is assumed to involve irreversible dislocation motion.

The vast majority of mechanical tests are not conducted in a discrete loading manner and hence the use of the onset of relaxation as a means of identifying initiation of slip for yield determination has not been envisioned. Initial localized deformation has been reported in studies of microplasticity using full-field strain analyses [45]. These observations have also been related to the non-linear portion of the global stress-strain curve, where the first observable localized strain is found at stress levels well above the elastic limit. In their work, Moulart and coworkers [45] attribute the inability to observe local deformation in the non-linear region as being related to "resolution limitations". Although not explicitly

stated, their findings are consistent with the notion of an onset of irreversible dislocation motion in localized regions of the microstructure. As in the present work, the more uniform anelastic strains would make it difficult to identify significant local strain in full field analysis for stresses in the non-linear regime just above the elastic limit, the point where applied stress leads to the activation of the earliest irreversible plastic deformation.

Summary and Concluding Remarks

We propose a new definition and a robust methodology to determine the onset of plastic flow in polycrystalline metals under increasing stress. This approach is independent of any measurement of strain or Young's modulus and is instead, based on the onset of stress relaxation. This new definition avoids the estimation of yield defined by an arbitrary offset in plastic strain, and the subjective determination obtained by approximating the stress value at the point of deviation from proportionality during initial loading. In fact, the OPRA stands in contrast to the elastic limit. It follows the accumulation of both elastic strain and anelastic, recoverable strain, as stress increases during loading of a polycrystalline metal. Since the lack of stress relaxation is indicative of an absence of dislocation motion, or other possible contributors to plastic deformation (e.g. twinning), the observation of an onset of stress relaxation is interpreted as a physics-based indicator of the onset of plastic flow. This conclusion is further supported by the absence of detectable, net irreversible strain upon unloading from stresses below our new OPRA definition of yielding. The present experiments take place under dislocation-plasticity dominated testing conditions for Cu and Mg. The determined OPRA yield point is independent of the magnitude of loading increment. The presence of an OPRA yield point is also supported by the presence of detectable irreversible net strain after unloading from stress states above the OPRA. Such non-recoverable strain occurs even for stress values well below the conventional 0.2 % offset yield point. Our experiments have shown that the proposed new methodology for yield determination is not subjective and therefore can be used to measure the true yield surface with no interference from anelastic or recoverable strains. The proposed designation can be applied a) at elevated temperatures and under harsh environments where strain measurement can be challenging and b) to other classes of materials such as hcp alloys (like Mg) where multiple unique slip systems exist, each exhibiting unique critical resolved shear stress values and where twinning can play an important role during deformation. At the same time, this OPRA definition of yield may introduce new challenges for modeling. In the case of Mg, results suggest that the stress state is not constrained to lie on the yield surface, which is currently an assumption of conventional plasticity.

Strain measurements cannot differentiate the elastic, anelastic and plastic contributions in order to detect this earliest dislocation activity. We show that stress measurements, on the other hand, can determine the earliest evidence of plastic flow with great sensitivity through the relaxation phenomenon. A yield point in the stress-strain response is difficult to distinguish near the elastic limit. If such a point is intended to identify the onset of irreversible dislocation slip activity, then the relaxation onset test proposed here is a powerful new probe of a materials underlying structure.

Finally, applicability of our new definition needs to be verified for other materials (such as microcracked ceramics [46–48], nanomaterials etc.) and in conditions where dislocation glide does not remain the dominant source of plastic deformation. For example, at higher temperatures, significant creep deformation and stress relaxation can occur at a small fraction of the traditionally defined yield stress. In such cases, one of two scenarios may emerge: (i) we may encounter the limits of our definition and they may be restricted to dislocation glide dominated conditions of plastic flow or (ii) a modification of the existing definition of yielding at elevated temperature may be required to accommodate time dependent plastic deformation related to any mechanism, e.g. creep by grain boundary sliding, bulk diffusion, etc. Additional application of the OPRA yield evaluation may prove valuable in other testing modes such as those in fatigue or high strain rate experiments. For example, knowledge of the lowest stress level needed to activate dislocation sources is central to evaluating fatigue lifetime. Currently, scale-up of OPRA tests are being considered for discrete loading experiments on bulk polycrystalline materials while the relaxation analyses may also have application to single crystal deformation experiments or to very small scale testing. OPRA should be equally effective in detecting plastic flow during compression loading for such tests. Activation of slip systems in these cases may be quite abrupt as available sources become rare and limited dislocation interactions influence localization of slip work hardening behavior.

Acknowledgments Research sponsored by the U.S Department of Energy, Office of Fossil Energy, Solid State Energy Conversion Alliance (SECA) Program. Some of the instruments used in this investigation, which are part of the High Temperature Materials Laboratory at ORNL had been acquired with support from the U.S Department of Energy's Vehicle Technologies Program.

References

1. Rajagopalan J, Han JH, Saif MTA (2007) Plastic deformation recovery in freestanding nanocrystalline aluminum and gold thin films. Science 315(5820):1831–1834
2. Hull D, Bacon DJ (1984) Introduction to dislocations, vol 257. Pergamon Press, Oxford
3. Dieter GE, Bacon D (1986) Mechanical metallurgy, vol 3. McGraw-Hill, New York

4. Kuhn H, Dana M (2000) ASM handbook mechanical testing and evaluation 8
5. Christensen RM (2008) Observations on the definition of yield stress. Acta Mech 196(3–4):239–244
6. Ashby MF, Cebon D (1993) Materials selection in mechanical design. J Phys IV 3(C7):C7–1
7. Zhou M (2013) Exceptional properties by design. Science 339(6124):1161–1162
8. Michno MJ, Findley WN (1976) An historical perspective of yield surface investigations for metals. Int J Non Linear Mech 11(1):59–82
9. Cleveland RM, Ghosh AK (2002) Inelastic effects on springback in metals. Int J Plast 18(5):769–785
10. Geng L, Shen Y, Wagoner RH (2002) Anisotropic hardening equations derived from reverse-bend testing. Int J Plast 18(5):743–767
11. Khan AS, Kazmi R, Pandey A, Stoughton T (2009) Evolution of subsequent yield surfaces and elastic constants with finite plastic deformation. Part-I: a very low work hardening aluminum alloy (Al6061-T6511). Int J Plast 25(9):1611–1625
12. Khan AS, Pandey A, Stoughton T (2010) Evolution of subsequent yield surfaces and elastic constants with finite plastic deformation. Part II: a very high work hardening aluminum alloy (annealed 1100 Al). Int J Plast 26(10):1421–1431
13. Khan AS, Pandey A, Stoughton T (2010) Evolution of subsequent yield surfaces and elastic constants with finite plastic deformation. Part III: yield surface in tension–tension stress space (Al 6061–T 6511 and annealed 1100 Al). Int J Plast 26(10):1432–1441
14. Phillips A (1986) A review of quasistatic experimental plasticity and viscoplasticity. Int J Plast 2(4):315–328
15. Phillips A, Das PK (1985) Yield surfaces and loading surfaces of aluminum and brass: an experimental investigation at room and elevated temperatures. Int J Plast 1(1):89–109
16. Naghdi PM, Essenberg F, Koff W (1958) An experimental study of subsequent yield surfaces in plasticity. J Appl Mech
17. Stout MG, Martin PL, Helling DE, Canova GR (1985) Multiaxial yield behavior of 1100 aluminum following various magnitudes of prestrain. Int J Plast 1(2):163–174
18. Uchic MD, Shade PA, Dimiduk DM (2009) Plasticity of micrometer-scale single crystals in compression. Annu Rev Mater Res 39:361–386
19. Miguel MC, Zapperi S (2006) Fluctuations in plasticity at the microscale. Science 312:1151–1152
20. Uchic MD, Dimiduk DM, Florando JN, Nix WD (2004) Sample dimensions influence strength and crystal plasticity. Science 305(5686):986–989
21. Dimiduk DM, Woodward C, LeSar R, Uchic MD (2006) Scale-free intermittent flow in crystal plasticity. Science 312(5777):1188–1190
22. Csikor FF, Motz C, Weygand D, Zaiser M, Zapperi S (2007) Dislocation avalanches, strain bursts, and the problem of plastic forming at the micrometer scale. Science 318(5848):251–254
23. Legros M, Gianola DS, Motz C (2010) Quantitative *in situ* mechanical testing in electron microscopes. MRS Bull 35(05):354–360
24. Liu HH, Schmidt S, Poulsen HF, Godfrey A, Liu ZQ, Sharon JA, Huang X (2011) Three-dimensional orientation mapping in the transmission electron microscope. Science 332(6031):833–834
25. Aifantis EC, Gerberich WW (1975) A theoretical review of stress relaxation testing. Mater Sci Eng 21:107–113
26. Meyers MA, Guimaraes JRC, Avillez RR (1979) On stress-relaxation experiments and their significance under strain-aging conditions. Metall Trans A 10(1):33–40
27. Lee D, Hart EW (1971) Stress relaxation and mechanical behavior of metals. Metall Trans 2:1245–1248
28. Gupta I, Li JCM (1970) Stress relaxation, internal stress, and work hardening in some BCC metals and alloys. Metall Trans 1(8):2323–2330
29. Hart EW, Solomon HD (1973) Load relaxation studies of polycrystalline high purity aluminium. Acta Metall 21(3):295–307
30. Hart EW (1970) A phenomenological theory for plastic deformation of polycrystalline metals. Acta Metall 18(6):599–610
31. Krempl E (1979) An experimental study of room-temperature rate-sensitivity, creep and relaxation of AISI type 304 stainless steel. J Mech Phys Solids 27(5):363–375
32. Law CC, Beshers DN (1972) Stress relaxation in fcc and hcp metals. Scr Metall 6(7):635–640
33. Povolo F (1981) On the analysis of stress relaxation data. J Nucl Mater 96(1):178–186
34. Gibbs GB (1966) Creep and stress relaxation studies with polycrystalline magnesium. Philos Mag 13(122):317–329
35. Hull D, Noble F (1964) Indirect measurements of the effect of stress on the velocity of dislocations. Discuss Faraday Soc 38:251–261
36. Guiu F (1969) On the measurement of internal stress by stress relaxation. Scr Metall 3(10):753–755
37. Lloyd DJ, Embury JD (1971) Stress relaxation testing and the determination of the internal stress. Phys Status Solidi B 43(1):393–399
38. Shade PA, Kim SL, Wheeler R, Uchic MD (2012) Stencil mask methodology for the parallelized production of microscale mechanical test samples. Rev Sci Instrum 83(5):053903
39. Wheeler R, Pandey A, Shyam A, Tan T, Lara-Curzio E (2015) Small scale mechanical characterization of thin foil materials via pin load microtesting. doi: 10.1007/s11340-015-0020-6
40. Pandey A, Tolpygo VK, Hemker KJ (2013) Thermomechanical behavior of developmental thermal barrier coating bond coats. JOM 65(4):542–549
41. Kammers AD, Daly S (2013) Digital image correlation under scanning electron microscopy: methodology and validation. Exp Mech 53(9):1743–1761
42. Phillips A, Sierakowski RL (1965) On the concept of the yield surface. Acta Mech 1(1):29–35
43. Sharpe WN Jr, Pulskamp J, Gianola DS, Eberl C, Polcawich RG, Thompson RJ (2007) Strain measurements of silicon dioxide microspecimens by digital imaging processing. Exp Mech 47(5):649–658
44. Frost H J, Ashby MF (1982) Deformation mechanism maps: the plasticity and creep of metals and ceramics
45. Moulart R, Rotinat R, Pierron F (2009) Full-field evaluation of the onset of microplasticity in a steel specimen. Mech Mater 41(11):1207–1222
46. Pandey A, Shyam A, Watkins TR, Lara-Curzio E, Stafford RJ, Hemker KJ (2014) The uniaxial tensile response of porous and microcracked ceramic materials. J Am Ceram Soc 97(3):899–906
47. Shyam A, Bruno G, Watkins TR, Pandey A, Lara-Curzio E, Parish CM, Stafford RJ (2015) The effect of porosity and microcracking on the thermomechanical properties of cordierite. J Eur Ceram Soc 35(16):4557–4566
48. Pandey A, Shyam A, Liu Z, Goettler R (2015) In-situ young's moduli of the constitutive layers in a solid oxide fuel cell. J Power Sources 273:522–529